ORIGINAL PAPER

Pharmacophore mapping of a series of pyrrolopyrimidines, indolopyrimidines and their congeners as multidrug-resistance-associated protein (MRP1) modulators

Nilesh R. Tawari · Seema Bag · Mariam S. Degani

Abstract Pharmacophore mapping studies were undertaken for a series of molecules belonging to pyrrolopyrimidines, indolopyrimidines and their congeners as multidrug resistance-associated protein (MRP1) modulators. A five-point pharmacophore with two hydrogen bond acceptors (A), one lipophilic/hydrophobic group (H), one positive ionic feature (P) and one aromatic ring (R) as pharmacophoric features was developed. The pharmacophore hypothesis yielded a statistically significant 3D-QSAR model, with a correlation coefficient of $r^2 = 0.799$ for training set molecules. The model generated showed excellent predictive power, with a correlation coefficient $Q^2 = 0.679$ for an external test set of 20 molecules. The pharmacophore was further validated using four structurally diverse compounds with MRP1 modulatory activity. These compounds mapped well onto four of the five features of the pharmacophore. The pharmacophore proposed here was then utilised for the successful retrieval of active molecules with diverse chemotypes from database search. The geometry and features of pharmacophore are expected to be useful for the design of selective MRP1 inhibitors.

Keywords Multidrug resistance-associated protein1 · Multidrug resistance · Pharmacophore mapping · 3D-QSAR

N. R. Tawari · S. Bag · M. S. Degani (✉)
Department of Pharmaceutical Sciences and Technology, Institute of Chemical Technology, University of Mumbai,
Matunga (E),
Mumbai 400019, India
e-mail: msdegani@udct.org

Introduction

The phenomenon of development of cross resistance by tumour cells treated with multiple chemotherapeutic agents is known as multidrug resistance (MDR). Cancer chemotherapy often fails due to the development of MDR. One form of MDR is caused by active efflux of drugs from tumour cells mediated by large polytopic membrane proteins. In humans, two ATP-binding cassette (ABC) transporters have been documented to cause resistance in tumour cells: P-glycoprotein (Pgp) (MDR1) and multidrug resistance-associated protein 1 (MRP1) [1, 2]. These transporters function by binding to drugs within the cell and releasing them into the extracellular space using energy from the hydrolysis of adenosine tri-phosphate (ATP). Tumour cells that are exposed to cytotoxic compounds often overexpress these efflux pumps, allowing such cells to survive even in the presence of anticancer agents. Overexpression of these proteins is well documented to occur in a number of tumour types, indicating that this mechanism of MDR is clinically important. Additionally, several studies have shown that expression of these proteins may be a prognostic indicator in certain malignancies [3].

Because of the importance of these proteins in clinical oncology, search for antagonists of these proteins, often called MDR modulators, has intensified. These antagonists function by blocking transporter-mediated drug efflux so that a concomitantly administered anticancer drug can cause tumour cell death. Initial efforts to develop MDR modulators were focussed mainly on verapamil and cyclosporin A. These compounds demonstrated excellent in vitro reversal of MDR but failed to achieve clinical success due to their intrinsic toxicity and/or alteration of the pharmacokinetics of the co-administered anticancer drugs.
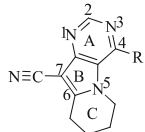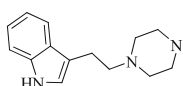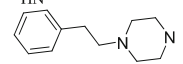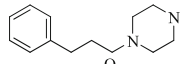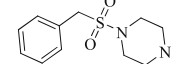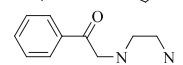
Many investigations report common structural features responsible for MDR1 modulation [4–11]. While several inhibitors of MDR1 have entered clinical trials, the development of specific MRP1 inhibitors remains in its infancy, although Eli Lilly has reported raloxifene analogues and isooxazoloquinoline analogues as selective MRP1 inhibitors [1]. Furthermore, little structure-activity relationship (SAR) data is available for selective MRP1 inhibitors. Touhey et al. [12] investigated the SAR of indomethacin mediated MRP-1 inhibition. Recently Ramaen et al. [13] reported the crystal structure of human MRP1 nucleotide binding domain 1. However, due to the lack of a complete crystal structure of MRP1, ligand-based drug design remains the major tool for rational drug design in this area. Cheng et al. performed pharmacophore mapping studies for several drug transporter proteins, including MRP1 [14]. Wang et al. [1, 2] reported studies on pyrrolopyrimidines, and templates derived from them, as novel and selective MRP1 inhibitors. Lather et al. [15] have described a topological model for the prediction of MRP1 inhibitory activity.

Ligand-based drug design approaches like pharmacophore mapping [16] and quantitative structure-activity relationship (QSAR) [17, 18] can be used in drug discovery in several ways, e.g. rationalisation of activity trends in molecules under study, prediction of the activity of novel compounds, and database search studies in search of new hits and to identify important features for activity. This paper describes the development of a robust ligand-based

Table 1 Compounds used in this study and their IC$_{50}$ values (μM)

Compound		R	IC$_{50}$
1.	(T)[a]	PhCH$_2$CH$_2$NH	6.3
2.		PhCH$_2$CH$_2$NCH$_3$	9.0
3.		PhCH$_2$SO$_2$NH	20.9
4.			0.6
5.			0.69
6.			7.35
7.	(T)		6.65
8.			1.85

Table 2 Compounds used in this study and their IC$_{50}$ values (μM)
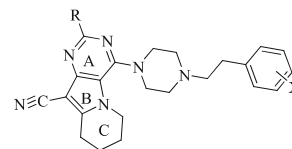
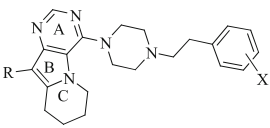| Compound	X	R	IC$_{50}$
9.	2-Cl	H	0.955
10.	3-Cl	H	0.920
11.	4-Cl	H	0.399
12. (T)	2-NO$_2$	H	1.415
13.	3-NO$_2$	H	0.410
14. (T)	4-NO$_2$	H	0.523
15.	3-MeO	H	2.300
16.	4-MeO	H	>50
17. (T)	3,4-F, F	H	0.229
18.	H	I	0.887
19. (T)	H	Ph	0.715
20.	H	4-CH$_3$CONHPh	0.570
21.	3,4-F, F	3-Pyr	0.218
22.	3,4-F, F	4-Pyr	0.105
23. (T)	3,4-F, F	2-CH$_3$-Ph	0.62

[a] T indicates compounds in the test set

3D-pharmacophore hypothesis using Pharmacophore Alignment and Scoring Engine (PHASE) for MRP1 [19]. The alignment obtained from the pharmacophoric points is used to derive an atom-based 3D-QSAR model. The pharmacophore thus developed imparts information about important features for MRP1 modulatory activity and geometry, and has the ability to mine 3D-virtual databases of drug-like molecules. Furthermore, the contours generated from QSAR studies highlight the structural features required for MRP1-mediated MDR modulatory activity, and is useful for further design of more potent inhibitors.

Methods

Biological data

A set of 80 compounds (shown in Tables 1–7) belonging to the family of pyrrolopyrimidines, indolopyrimidines and their congeners and reported as selective MRP1 inhibitors [1, 2] were used for pharmacophore generation. The

Table 3 Compounds used in this study and their IC$_{50}$ values (μM)

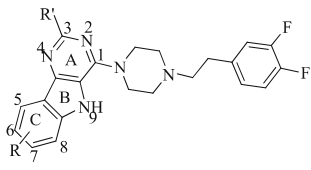| Compound	X	R	IC$_{50}$
24. (T)	H	H$_3$C—CO— (acetyl)	2.800
25.	H	phenyl—CO— (benzoyl)	1.370
26. (T)	H	H$_3$C—O—CO—O—	0.910
27.	H	methyl-thiazole	0.533
28.	H	methyl-oxadiazole	0.650
29.	H	pyrimidinyl	0.675
30.	3,4-F, F	-CONH$_2$	0.138
31.	3,4-F, F	-CONH Et	0.120
32.	3,4-F, F	dimethoxybenzyl-NH-CO-	0.0430
33. (T)	3,4-F, F	pyridyl-methyl-NH-CO-	0.061
34. (T)	3,4-F, F	pyridyl-NH-CO-	0.076

activity of all compounds used in the QSAR study was reported to have been measured by drug accumulation assay using the MRP1-expressing cell line COR.L23/R, and is reported as IC$_{50}$ for daunomycin accumulation, where 100% accumulation is that observed in the presence of a known MRP1 modulator: verapamil at 100 μM [1, 2]. The negative logarithm of the measured IC$_{50}$ value (pIC$_{50}$) was used in the 3D-QSAR study. These 80 compounds were divided into a training set (60 compounds) and a test set (20 compounds) using randomisation as well as chemical and biological diversity.
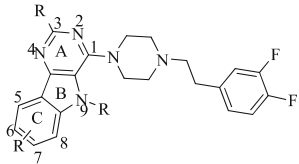
Generation of common pharmacophore hypothesis

The common pharmacophore hypothesis (CPH) and alignment based on it was carried out using PHASE, version 2.0, 2006 (Schrödinger, LLC, New York, NY) installed on an AMD Athelon workstation [20]. The structures were imported from the project table in the "Develop Pharmacophore Hypothesis" panel and geometrically refined (cleaned) using Ligprep. Conformations were generated by the MCMM/LMOD method using a maximum of 2,000 steps with a distance-dependent dielectric solvent model
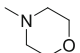
and an OPLS-2005 force field. All the conformers were subsequently minimised using truncated Newton conjugate gradient minimisation up to 500 iterations. For each molecule, a set of conformers with a maximum energy difference of 30 kcal/mol relative to the global energy minimum conformer was retained. A redundancy check of 2 Å in the heavy atom positions was applied to remove duplicate conformers. Pharmacophore features—hydrogen bond acceptor (A), hydrogen bond donor (D), hydrophobic group (H), negatively charged group (N), positively charged group (P), aromatic ring (R)—were defined by a set of chemical structure patterns as SMARTS queries and assigned one of three possible geometries that define the physical characteristics of the site:

1. Point—the site is located on a single atom in the SMARTS query.

Table 4 Compounds used in this study and their IC$_{50}$ values (μM)

Compound	R	R'	IC$_{50}$
35.	5-CH$_3$	H	1.235
36. (T)	6-NO$_2$	H	0.133
37.	6-MeO	H	0.820
38.	6-NHCOCH$_3$	H	2.710
39.	6-COCH$_3$	H	0.113
40.	6-CONH$_2$	H	3.440
41.	6-SO$_2$N-pyrrolidine	H	0.235
42.	5-Cl	H	0.367
43.	5-CN	H	0.277
44.	5-CONH$_2$	H	0.183
45.	5-CONHPy-4	H	0.650
46. (T)	5-NO$_2$	H	0.183
47.	5-NH$_2$	H	1.900
48.	7-MeO	H	3.150
49.	7-MeO, 8-NO$_2$	H	3.45
50.	5-NO$_2$, 6-MeO	H	0.078

Table 5 Compounds used in this study and their IC$_{50}$ values (μM)

Compound	R	R$_1$	R$_2$	IC$_{50}$
53.	5-NO$_2$	CH$_3$	H	0.147
54.	5-NO$_2$	Ph(CH$_2$)$_2$	H	0.222
55.	5-NO$_2$	CH$_2$Py-3	H	0.621
56.	5-NO$_2$	CH$_2$Py-4	H	0.080
57.	5-CONH$_2$	CH$_3$	H	0.062
58. (T)	5-CONH$_2$	CH$_2$COEt	H	0.122
59. (T)	5-CONH$_2$	CH$_2$Py-4	H	0.270
60.	6-NO$_2$	CH$_2$COEt	H	0.138
61.	5-CONH$_2$	CH$_3$	*(morpholine group)*	0.230

2. Vector—the site is located on a single atom in the SMARTS query, and assigned directionality according to one or more vectors originating from the atom.
3. Group—the site is located at the centre of a group of atoms in the SMARTS query. For aromatic rings, the site is assigned directionality, defined by a vector that is normal to the plane of the ring.

Active and inactive thresholds of pIC$_{50}$ of 7.00 and 5.50, respectively, were applied to the dataset (Tables 1–7) to yield 12 actives and 7 inactives that were used for pharmacophore generation and subsequent scoring. Common pharmacophoric features were then identified from a set of variants—a set of feature types that define a possible pharmacophore—using a tree-based partitioning algorithm with maximum tree depth of four with the requirement that all 12 actives must match. The final size of the pharmacophore box was 1 Å to optimise the number of final CPHs. These CPHs were examined using a scoring function to yield the best alignment of the active ligands using an overall maximum root mean square deviation (RMSD) value of 1.2 Å with default options for distance tolerance. The quality of alignment was measured by a survival score, defined as:

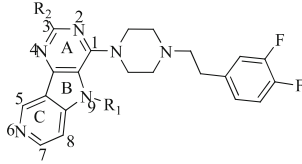$$S = W_{site}S_{site} + W_{vec}S_{vec} + W_{vol}S_{vol} + W_{sel}S_{sel}$$
$$+ W_{rew}^m \qquad (1)$$

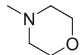Where W are weights and S are scores; S_{site} represents alignment score, the RMSD in the site point position; S_{vec} represents vector score, and averages the cosine of the angles formed by corresponding pairs of vector features in aligned structures; S_{vol} represents volume score based on overlap of van der Waals models of non hydrogen atoms in each pair of structures; and S_{sel} represents selectivity score, and accounts for what fraction of molecules are likely to match the hypothesis regardless of their activity towards the receptor.
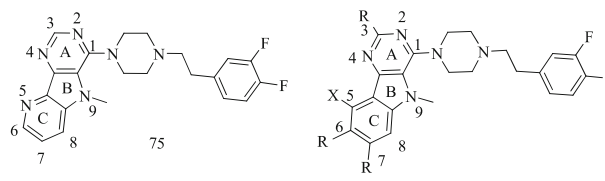
W_{site}, W_{vec}, W_{vol}, W_{rew} have default values of 1.0, while W_{sel} has a default value of 0.0. In hypothesis generation, default values have been used. W_{rew}^m represents reward weights defined by $m-1$ where m is the number of actives that match the hypothesis.
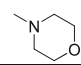
QSAR model building

A training set of 60 molecules was selected randomly, incorporating biological and chemical diversity, and was used to generate atom-based QSAR models for all hypotheses using a grid spacing of 1.0 Å. Models containing four or more partial least squares (PLS) factors tended to fit the pIC$_{50}$ values beyond their experimental uncertainty, therefore only one, two and three factor models were considered. Each of these models was validated using

Table 6 Compounds used in this study and their IC$_{50}$ values (μM)

Compound	R	R$_1$	R$_2$	IC$_{50}$
62.	H	CH$_3$	H	0.044
63. (T)	H	CH$_2$Ph	H	0.545
64.	5-Cl	CH$_3$	H	0.130
65.	5-MeO	CH$_3$	H	0.172
66.	5-^{i}PrO	CH$_3$	H	0.265
67.	5-NMe$_2$	CH$_3$	H	0.166
68.	5-NHMe	CH$_3$	H	0.115
69.	5-NHCH$_2$Py-2	CH$_3$	H	0.106
70.	morpholine	CH$_3$	H	0.071
71.	5-CH$_3$	CH$_3$	H	0.033
72.	7-Cl	CH$_3$	H	1.200
73. (T)	5-Cl	CH$_3$	CH$_2$OMe	0.244
74.	5-Cl	CH$_3$	*(morpholine group)*	0.090

Table 7 Compounds used in this study and their IC$_{50}$ values (μM)

Compound	R$_1$	R$_2$	R$_3$	X	IC$_{50}$
75.					0.270
76.	H	H	H	CN	0.355
77. (T)	CH$_3$	H	H	CN	1.255
78.	CH$_3$	H	H	CONH$_2$	0.223
79. (T)	H	H	H	CONH$_2$	0.110
80. (T)	CH$_3$	NO$_2$	H	CONH$_2$	0.088
81.	H	H	(morpholine)	CONH$_2$	0.097

[a](T) indicates compounds in the test set

an external test set of 20 molecules that were not considered during model generation.

Validation of the generated pharmacophore

The generated pharmacophore model was used to carry out a search of the ASINEX (http://zinc.docking.org/vendor0/asin/index.html asin_p0.0.sdf) database version 2006.3, # in catalog: 372187 made up of 45,533 molecules seeded with four highly active molecules belonging to different chemotypes and three inactives for MRP1-mediated MDR modulatory activity. The minimum criteria for retrieval of hits was that four out of five pharmacophoric features must match, with default tolerance on matching the pharmacophore feature to each of the five inter-feature distances. The molecules were minimised using Ligprep and a maximum of 100 conformers were generated for these molecules using the ligand torsional search method.

Results and discussion

Pharmacophore models containing three, four and five sites were generated using a terminal box size of 1 Å with 12 highly active molecules, belonging to pyrrolopyrimidines, indolopyrimidine and their congeners, selected using a tree based partition algorithm from the publications of Wang et al. [1, 2]. The three- and four-featured CPHs were rejected, as they were unable to define the complete binding space of the selected molecules. A total of 38,482 probable five-featured

CPHs belonging to 10 types (AAHHH, AHHRR, AAHPR, AHHHR, AHPRR, AAHPR, AHHHP, AAHRR, AAHHP and AAHHR) were subjected to stringent scoring function analysis with respect to actives using default parameters for site, vector, and volume. Reference relative conformational energy (kJ/mol) was included in the score with a weight of 0.01, and ligand activity, expressed as pIC$_{50}$, was incorporated with a weight of 1.0. Hypotheses emerging from this process were subsequently scored with respect to the seven inactives, using a weight of 1.0. The hypotheses that survived the scoring process were used to build an atom-based QSAR model. A summary of statistical data of the best CPHs, labeled CPH1 to CPH6, with their survival scores is listed in Table 8.

Good and consistent external predictivity was observed for CPH1 for each combination as compared to the others. CPH1 showed a good r^2 value for the training set (0.799) and excellent predictive power with Q^2 of 0.679. A good Pearson-R value of 0.883 was also observed. Actual and predicted values of the training set and test set molecules are given in the Electronic Supplementary Material. Other pharmacophore models with good statistics (Table 8) were not able to map diverse chemotypes having MRP1-mediated MDR modulatory activity. Hence, the hypothesis CPH1 with two hydrogen bond acceptors (A), one lipophilic/hydrophobic group (H), one positive ionic feature (P) and one aromatic ring (R) as pharmacophoric features was retained for further studies. Figure 1 shows the alignment of the molecules under study along with CPH1. The distances and angles between the pharmacophoric features are depicted in Fig. 2a and b, respectively. Figure 3 shows the graphs of actual vs predicted activity for training and test set molecules. The pharmacophore contains two acceptor features mapping on the lone pair of vectors of two nitrogen atoms in the pyrimidine ring, one aromatic ring feature mapping on the pyrrole heterocycle, one positive ionic feature mapping on one of the nitrogens in the piperazine ring, and one lipophilic/ hydrophobic feature mapping on the para-fluoro atom in the distal part of molecule.

Validation of the generated pharmacophore

The database search studies retrieved all the positive hits and filtered out two inactives. Interpretation of how the pharmacophore maps onto the positive hits can provide an insight into the structural requirements for MRP1-mediated MDR modulatory activity, and can act as a guide for further modification of the molecules. However, the actual activities of these compounds were not compared with the predicted activity since the activities of these compounds were measured by different assay methods; moreover, these compounds are significantly diverse from the compounds that were used to build the QSAR model, and hence occupy different chemical space, so the local QSAR model may not

Table 8 Summary of quantitative structure-activity relationship (QSAR) results for six best common pharmacophore hypotheses (CPHs) with survival scores. *SD* Standard deviation of the regression, r^2 value of r^2 for the regression, *F* variance ratio, *P* significance level of variance ratio, *RMSE* root-mean-square error, Q^2 value of Q^2 for the predicted activities, *Pearson-R* Correlation between the predicted and observed activity for the test set

|	CPH1(AAHPR)	CPH2 (AAHHH)	CPH3(AAHHP)	CPH4(AAHHR)	CPH5(AAHRR)	CPH6(AHHRR)
Survival score	10.837	10.311	10.819	11.025	10.777	10.875
SD	0.279	0.299	0.306	0.273	0.276	0.318
r^2	0.799	0.768	0.758	0.807	0.803	0.739
F	74.2	61.9	58.3	78.1	76.1	52.9
P	1.688e–19	8.67e–18	3.106e–17	5.368e–20	9.509e–20	2.353e–16
RMSE	0.347	0.406	0.353	0.352	0.369	0.369
Q^2	0.679	0.558	0.666	0.667	0.637	0.636
Pearson-R	0.833	0.777	0.827s	0.819	0.808	0.799

give the correct interpretation. Four highly active molecules —LY329146, LY402913, dehydrosilybin (DHS) and phenoxymethylquinoxalinone—that show MRP1-mediated MDR activity, were taken from a review of Boumendjel et al. [21, and references therein]. Figure 4 shows the chemical structure of these diverse MRP1-mediated MDR modulators used for validation of CPH1.

Eli Lilly has reported a raloxifene analogue, LY329146, which was able to reverse doxorubicin resistance in the MRP1-expressing HL60/ADR cell line. The two acceptors mapped to the two sulfonamide groups and the aromatic ring feature of the pharmacophore mapped to the benzene ring. The positive ionic feature mapped to the tertiary nitrogen of the piperidine ring system. However, LY329146 was unable to map onto the hydrophobic feature. Figure 5a

shows the mapping of LY329146 on CPH1. Thus, four out of five features were mapped on LY329146. This mapping indicates that substitution of a hydrophobic group on the piperidine ring, which can extend to the hydrophobic feature, may enhance the activity of the molecule. This information could provide a clue for the further modification of LY329146.

The isoxazole derivative LY402913 was reported by Eli Lilly to be a selective and potent MRP1-mediated MDR modulator. One acceptor feature of the pharmacophore mapped to the oxygen atom in the isoxazole ring, and the other acceptor to the carbonyl group. The aromatic ring feature mapped to the ring attached to isoxazole, the hydrophobic group mapped to the methyl group. However, the molecule was unable to map the positive ionic feature.

Fig. 1 Common pharmacophore hypothesis 1 (CPH1)-based alignment of multidrug resistance-associated protein (MRP) inhibitors
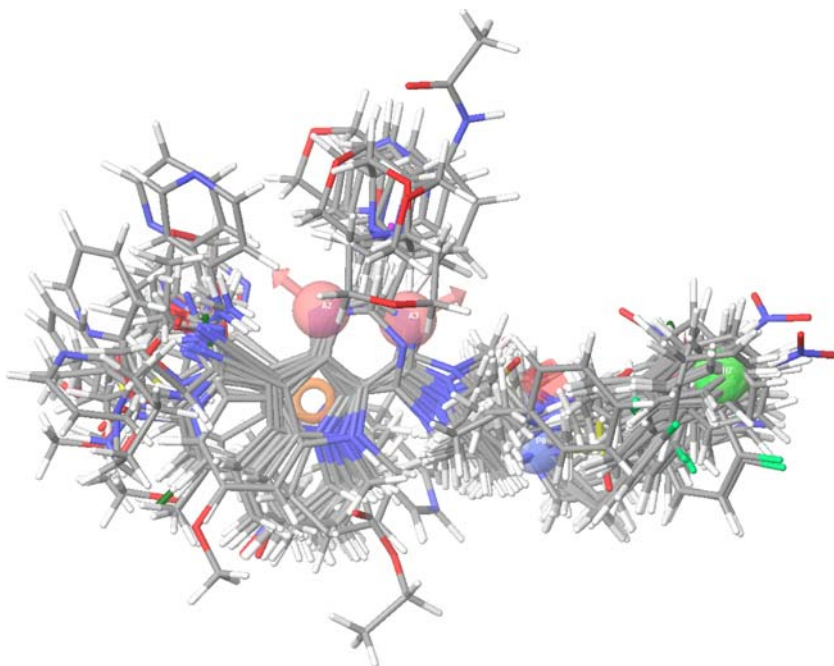
Fig. 2a,b Geometry of the pharmacophore. *Red spheres with vectors* Acceptor feature, *orange torus* aromatic ring feature, *blue sphere* positive ionic feature, *green sphere* hydrophobic feature. **a** CPH1 features and distances. **b** CPH1 features and angles
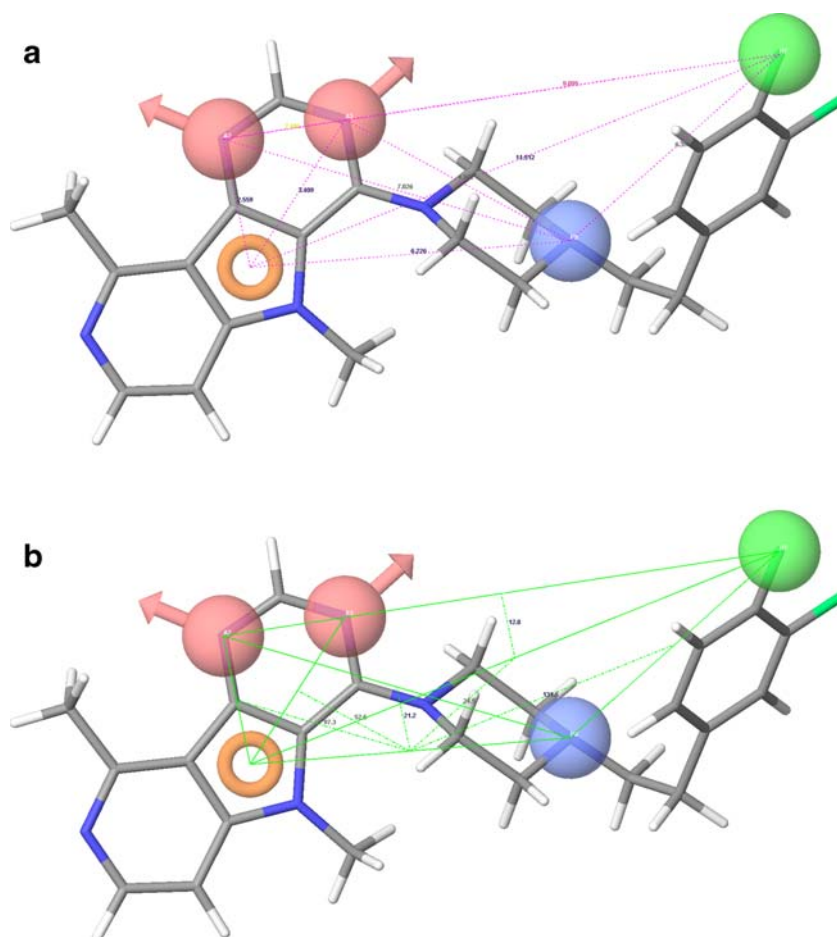

Figure 5b shows the mapping of LY402913 on CPH1. The mapping studies indicate that one positive ionic feature in the spacer part of the molecule might enhance MRP1 modulatory activity.

In the case of the flavonoid derivative DHS, the oxygen of the hydroxy group and the carbonyl group mapped on two acceptor features. The aromatic ring feature mapped on the benzene ring and the hydrophobic feature mapped on the methyl group. But DHS was unable to map to the positive ionic feature. Figure 5c shows the mapping of DHS on CPH1.

The oxygen of methoxy group and carbonyl group mapped onto the two acceptor features of the pharmacophore in phenoxymethylquinoxalinone. The aromatic ring feature and hydrophobic feature mapped on the two benzene rings. However, phenoxymethylquinoxalinone was unable to map on the positive ionic feature, which indicates room for chemical modification to improve activity. Figure 5d shows the mapping of phenoxymethylquinoxalinone on CPH1.

Thus, pharmacophore mapping studies carried out for further validation can be utilised for the chemical modification of different chemotypes with MRP1-mediated MDR

modulatory to improve their activity. Furthermore, these studies provide confidence in the applicability of the model for diverse chemotypes and its usefulness for 3D-database searching studies.
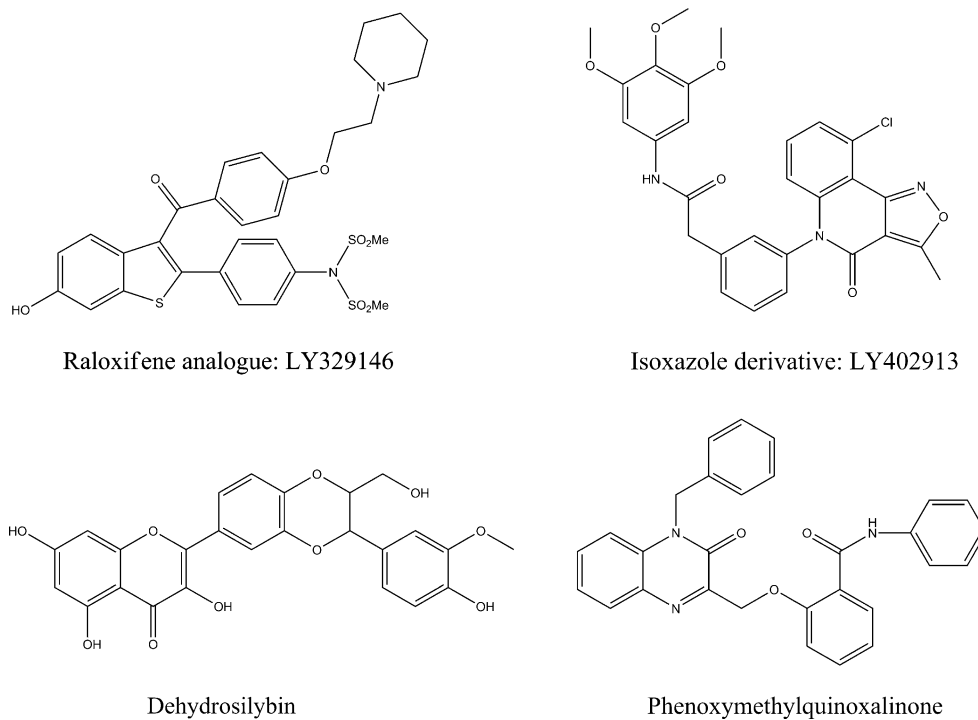
Interpretation of QSAR models

Additional insights into the inhibitory activity can be gained by visualising the QSAR model in the context of one or more ligands in the series with varying activity. This information can then be used to design new, more active analogues. A pictorial representation of the contours generated is shown in Fig. 6a–f. In these representations, the blue cubes indicate favourable regions while red cubes indicate unfavourable regions for activity.

Figure 6a and b compare the QSAR model in the context of the hydrogen bond donor property for the more active molecule 32 and the less active molecule 38. The blue regions were observed near the 7th position of pyrrolopyr-imidine compounds, thus molecules (30, 31, 32, 33 and 34) with a potential hydrogen bond donor at this position showed high activity (Fig. 6a). Red regions were observed near the N–H in the indolopyrimiding ring and hydrogen
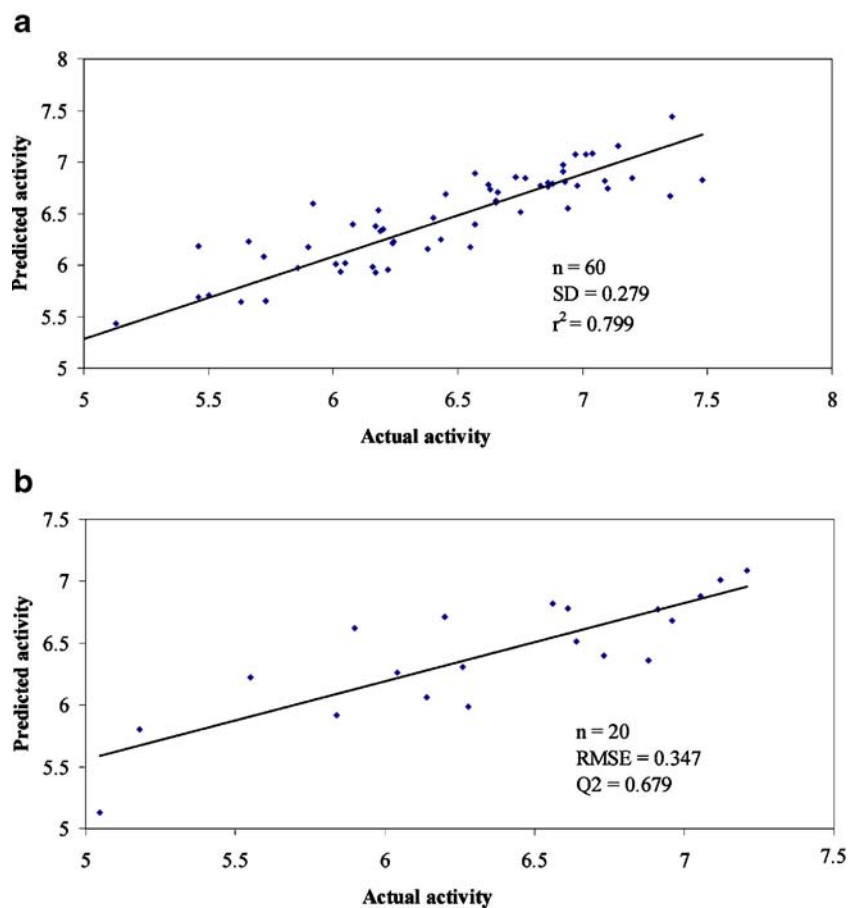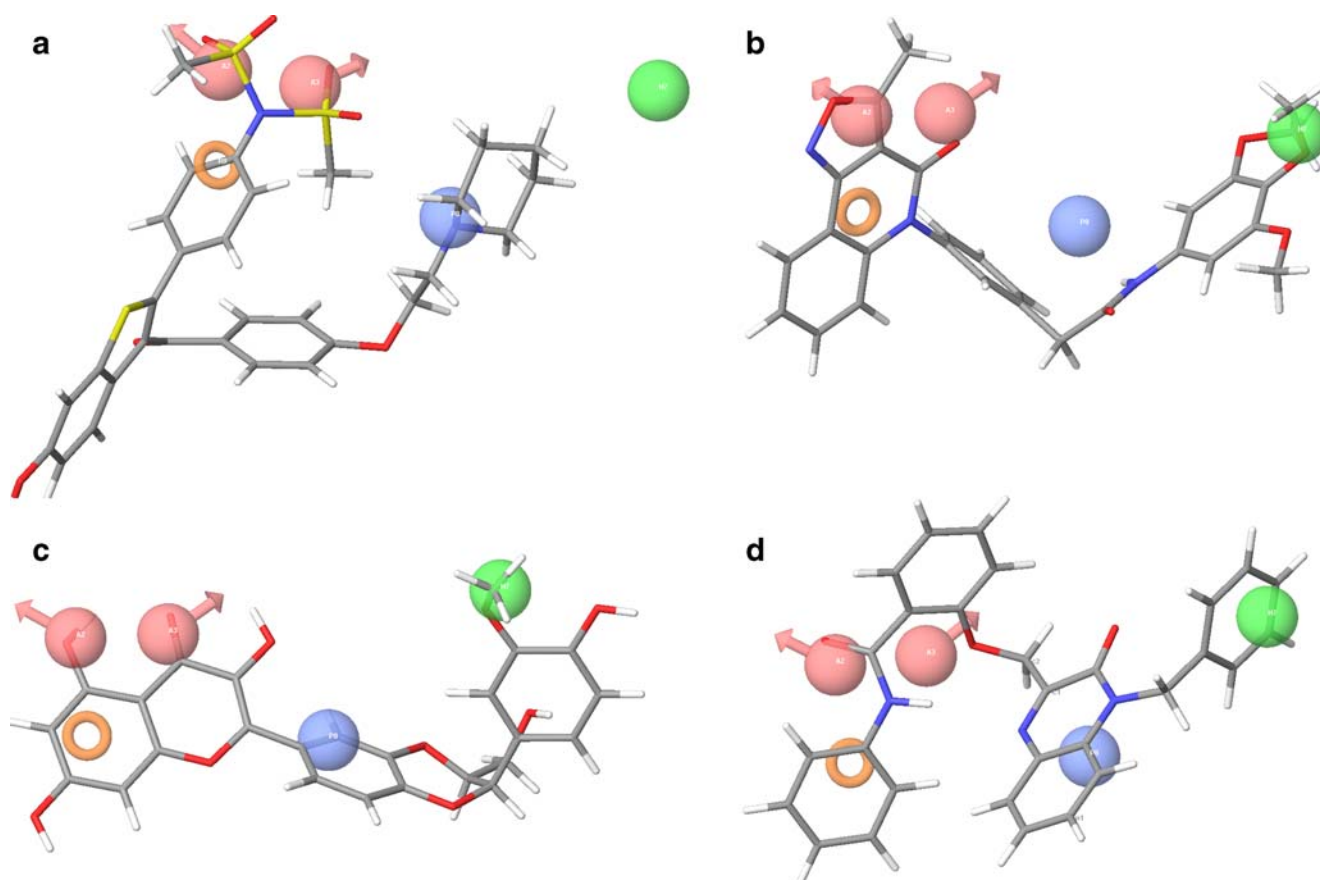
Fig. 3 Scatter plots for the predicted and experimental pIC_{50} values for the MRP1 QSAR model applied to the training set (**a**) and the test set (**b**); $r^2 = 0.799$, $Q^2 = 0.679$ and Pearson-R $= 0.883$

Fig. 4 The chemical structure of the four chemotypes showing MRP1-mediated MDR modulators used for validation of CPH1

Raloxifene analogue: LY329146

Isoxazole derivative: LY402913

Dehydrosilybin

Phenoxymethylquinoxalinone

Fig. 5 Mapping of compounds LY329146 (**a**), LY402913 (**b**), dehydrosilybin (DHS) (**c**) and phenoxymethylquinoxalinone (**d**) on CPH1 on the pharmacophore (colour codes as in Fig. 2)

bond donor substitution at the 6th position of ring C as in molecule 38 and 40, contributing to the lower activity of these molecules (Fig. 6b).

Figure 6c illustrates the significant favourable and unfavourable hydrophobic interactions that arise when the QSAR model is applied to the reference ligand 71—the most active compound in the training set (pIC$_{50}$=7.48). Blue regions were observed near the fluorine atom, which appears to be one of the pharmacophoric features. Further, more pronounced blue regions were visible near the two carbon linker and the phenyl ring that is present in all the most active ligands, thus making these features important for activity despite the fact that these features are missing from the pharmacophore. Blue regions near the ring C of the indolopyrimidine system and substitution at the 5th position (Tables 4, 5, 6, 7) indicate their importance for activity although these features are missing from the developed pharmacophore model.

A striking observation was that there are only a few unfavourable red regions in the case of the reference ligand, which is the most active molecule in the series. However, in the context of one or more inactive ligands, the QSAR

model can provide information about structural features that may be detrimental to activity [19]. For example, Fig. 6d shows a clear predominance of unfavourable interactions for the most inactive training set molecule, 2. In particular, the ring C protrudes significantly out from the indolopyrimidine ring system of the reference ligand, with a concomitant increase in the unfavourable volume compared to the reference ligand, justifying the possibility of reduced activity due to steric factors. Moreover, the phenyl ring attached to pyrrolopyrimidines system protrudes significantly away from the reference ligand, contributing to loss of activity. Thus, Fig. 6c and d compare the most significant favourable and unfavourable steric interactions that arise when the QSAR model is applied to the most (71) and least (2) active molecules.

Figure 6e and f compare the most significant favourable and unfavourable hydrogen bond acceptor and electron withdrawing features that arise when the QSAR model is applied to the most active molecule, 71 and 49 having intermediate activity. Blue regions were observed near the tertiary nitrogens, indicating their importance for activity.
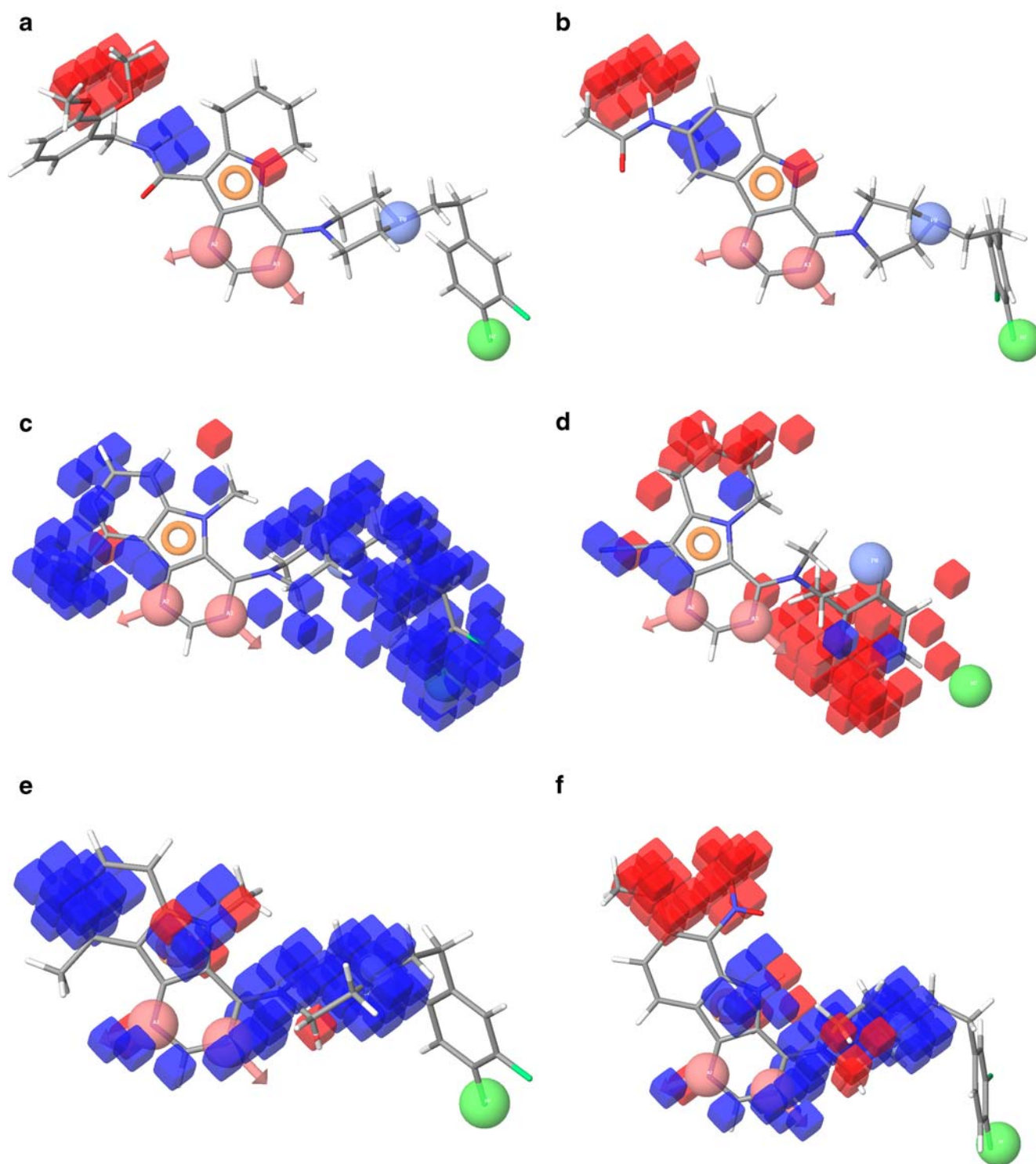
Fig. 6 Pictorial representation of the contours generated using the QSAR model. *Blue cubes* indicate favourable regions while *red cubes* indicate unfavourable region for the activity. **a** QSAR model visualised in the context of hydrogen bond donor property with molecule 32. **b** QSAR model visualised in the context of hydrogen bond donor property with molecule 38. **c** The significant favourable and unfavourable hydrophobic interactions that arise when the QSAR model is applied to reference ligand 71. **d** The significant favourable and unfavourable hydrophobic interactions that arise when the QSAR model is applied to the least active ligand, 2. **e** QSAR model visualised in the context of hydrogen bond acceptor property and electron withdrawing features with reference ligand 71. **f** QSAR model visualised in the context of hydrogen bond acceptor property and electron withdrawing features with ligand 49

Of these, two nitrogens in the pyrimidine ring and one nitrogen of the piperazine ring are also mapped as pharmacophoric features. In the case of ligands 48 and 49, red regions were associated with electron withdrawing groups at the 7th and 8th (Table 4) position, thereby leading to a decrease in activity (Fig. 6f).

Conclusions

Different pharmacophore hypotheses were developed using PHASE, and the alignment based on these pharmacophores was used as the input for the development of 3D-QSARs. A five-point pharmacophore with two hydrogen bond acceptors (A), one lipophilic/hydrophobic group (H), one positive ionic feature (P) and one aromatic ring (R) as pharmacophoric features was associated with the most significant QSAR model. Pharmacophore mapping studies provided an insight into the inhibitory potential of different chemotypes as MRP1-mediated MDR modulatory activity. Furthermore, visualisation of the 3D-QSAR model in the context of the molecules under study provided details of the relationship between structure and activity, and thus provides information regarding structural modifications with which to design analogues with better activity prior to synthesis.

In summary, in the absence of a crystal structure of the MRP1 receptor and knowledge of bioactive conformations of molecules, the ligand-based model presented in this study based on pharmacophoric conformations could be very useful for the design of better analogues. Moreover, the pharmacophore developed can be used as a 3D-query for virtual databases in the search for new MRP1 modulators.

References

1. Wang S, Folkers A, Chuckoweree I, Cockcroft X, Sohal S, Miller W, Milton J, Wren SP, Vicker N, Depledge P, Scott J, Smith L, Hazel J, Mistry P, Faint R, Thompson D, Cocks S (2004) J Med Chem 47:1329–1338
2. Wang S, Wan NC, Harrison J, Miller W, Chuckowree I, Sohal S, Hancox TC, Baker S, Folkes A, Wilson F, Thompson D, Cocks S, Farmer H, Boyce A, Freathy C, Broadbridge J, Scott J, Depledge P, Faint R, Mistry P, Charlton P (2004) J Med Chem 47:1339–1350
3. Lomovskaya O, Watkins W (2001) Curr Med Chem 8:1699–1791
4. Kim HK (2001) Bioorg Med Chem 9:1517–1523
5. Wiese M, Pajeva KI (1998) Quant Struct Act Relat 17:301–312
6. Wiese M, Pajeva KI (2001) Quant Struct Act Relat 20:130–138
7. Christoph G, Pajeva KI, Wiese M (2006) Bioorg Med Chem 14:1588–1598
8. Sarshar S, Zhang C, Moran EJ, Krane S, Rodarte JC, Benbatoul KD, Dixon R, Mjalli AMM (2000) Bioorg Med Chem Lett 10:2599–2601
9. Zhang C, Sarshar S, Moran EJ, Krane S, Rodarte JC, Benbatoul KD, Dixon R, Mjalli AMM (2000) Bioorg Med Chem Lett 10:2603–2605
10. Tsakovska MI (2003) Bioorg Med Chem 11:2889–2899
11. Labrie P, Maddaford SP, Fortin S, Rakhit S, Kotra LP, Gaudreault RC (2006) J Med Chem 49:7646–7660
12. Touhey S, O'Connor R, Plunkett S, Maguire A, Clynes M (2002) Eur J Cancer 38:1661–1670
13. Ramaen O, Leulliot N, Sizun C, Ulryck N, Pamlard O, Lallemand JY, Van Tilbeurgh H, Jacquet E (2006) J Mol Biol 359:940–949
14. Cheng C, Sean E, Bahadduri P, Swaan PW (2006) Adv Drug Deliv Rev 58:1431–1450
15. Lather V, Madan AK (2005) Bioorg Med Chem Lett 15:4967–4972
16. Narkhede SS, Degani MS (2007) QSAR Comb Sci 26:744–753
17. Vepuri S, Tawari NR, Degani MS (2007) QSAR Comb Sci 26:204–214
18. Ramar S, Bag S, Tawari NR, Degani MS (2007) QSAR Comb Sci 26:608–617
19. Dixon SL, Smondyrev AM, Knoll EH, Rao SN, Shaw DE, Friesner RA (2006) J Computer-Aided Mol Des 20:647–671
20. Phase, version 2.0 (2006) User manual. Schrödinger, LLC, New York, NY
21. Boumendjel A, Baubichon-Cortay H, Trompier D, Perrotton T, DPietro A (2005) Med Res Rev 25:453–472